# Target Detection in Unfocused SAR/ISAR Images: A Geometric Approach

Chuang He and José M. F. Moura
Department of Electrical and Computer Engineering
Carnegie Mellon University
Pittsburgh, PA 15213-3890

*Abstract*— **In synthetic aperture radar (SAR) and inverse synthetic aperture radar (ISAR), targets with uncompensated motion are blurred in the range-Doppler radar image. Our goal with this paper is twofold: 1) to analyze the image formation process in SAR/ISAR and develop a model for the distortion introduced by inadequate motion compensation; 2) to design a detection scheme that is robust to the smearing effects caused by inadequate motion compensation. We show that the blurring is equivalently modeled by describing the uncompensated target image as the superposition of space shifted echoes of a fully compensated target image. We then extend to the two-dimensional (2D) model, a geometrically based robust detection scheme we developed for the one-dimensional (1D) case. In this paper, we will describe the structure and the design of the 2D robust detector in detail.**

## I. Introduction

In synthetic aperture radar (SAR) and inverse synthetic aperture radar (ISAR), the relative motion between the radar platform and the target generates the spatial diversity needed to achieve the azimuth resolution. However, with high resolution SAR/ISAR systems, it is increasingly difficult to fully compensate for the relative motions. With 1m, or even higher, resolution radars becoming available, it is hard to assign a scatterer to a location when the scatterer changes its relative position within the synthetic aperture interval. This problem is known as the motion through resolution cell (MTRC) problem [1]. The net result of MTRC is that the range-Doppler image is blurred with loss of resolution. Computationally intensive image formation algorithms are needed to compensate for the MTRC effect. In general, these image formation algorithms require costly Fourier transform domain non-uniform interpolation which prohibits the real time processing of SAR/ISAR images.

This work was partially supported by DARPA through AFOSR grant # F49620-96-1-0436.

0-7803-3731-X/97$10.00©1997

In this paper, we first demonstrate that the blurring and smearing of the SAR/ISAR images due to MTRC is equivalently modeled by describing the uncompensated image of a target as the superposition of multiple space shifted echoes of the fully compensated target image. Then, we design a detector that is robust to multiple echoes with arbitrary space shifts. The idea is to include these distortions explicitly in the model, rather than ignoring them.

We use a geometrically based approach. The one-dimensional (1D) version of the algorithm is detailed in [2], [3]. In this paper, we extend the approach to the two-dimensional (2D) case. We define the signal subspace $\mathcal{S}$ as the set where the typical distorted target signatures lie in the SAR/ISAR image plane. The ideal robust target detector is matched to this signal subspace $\mathcal{S}$. In practice, this is too costly to implement. Our strategy is to design a representation subspace $\mathcal{G}$ close to the signal subspace $\mathcal{S}$ but such that the detector matched to $\mathcal{G}$ is easy to implement. The closeness between $\mathcal{S}$ and $\mathcal{G}$ is measured by the gap metric. The new robust detector is easy to implement and since it is an approximation of the ideal detector, it provides better performance than other simple detectors.

## II. Distortion model

In this section, we describe briefly the SAR/ISAR image formation process. The intent is to show that, for example, for a single point scatterer, the MTRC blurring that occurs can be modeled by describing the image of the scatterer as the superposition of space shifts of a fully focused image of the scatterer. Here, we concentrate our discussion on spotlight SAR. Specifically, we consider the distortion introduced by using the rectangular format algorithm (RFA) with a large synthetic aperture in spotlight mode.

### A. SAR image formation using RFA in spotlight mode

We will follow the notation in [1] assuming a point scatterer. The transmitted signal radar is

$$s_t(n,t) = A_0 \,\mathrm{rect}(\frac{\hat{t}}{T_p}) \exp\{j[2\pi f_c t + \pi\gamma\hat{t}^2]\} \quad (1)$$

where $n$ is the pulse index, $\hat{t} = t - nT$ is the fast time of pulse $n$, $T$ is the pulse repetition time, $T_p$ is the duration of the pulse, $c$ is the speed of light, $f_c$ is the carrier frequency, and $\gamma$ is the chirp rate. The signal component of the return is

$$\begin{aligned} s_r(n,t) &= a_t \,\mathrm{rect}(\frac{\hat{t}-t_d}{T_p}) \times \\ &\quad \exp\{j[2\pi f_c(t-t_d) + \pi\gamma(\hat{t}-t_d)^2]\} \quad (2) \end{aligned}$$

where $t_d = 2R_t/c$ and $R_t$ is the range from the SAR sensor to the scatterer.

After dechirping, omitting the higher order terms and approximating $R_t - R_0 \cong K(\dot{R}_t - \dot{R}_0)n$, $K$ is a constant, we get

$$\begin{aligned} s_{if}(n,t) &\cong a_t' \,\mathrm{rect}(\frac{\hat{t}-2R_t/c}{T_p}) \times \\ &\quad \exp\{-j\beta n\} \exp\{-j\alpha\hat{t}\} \quad (3) \end{aligned}$$

where $\beta = \frac{4\pi f_c K}{c}(\dot{R}_t - \dot{R}_o)$, $\alpha = \frac{4\pi\gamma}{c}(R_t - R_o)$, and $R_o$ is the range from the radar platform to the scene center.

Ideally, if $R_t - R_o$ and $\dot{R}_t - \dot{R}_o$ are constant over the synthetic aperture interval, then (3) is indeed a 2D Fourier transform of the image of a point scatterer. Thus, by taking the inverse Fourier transform of (3), we obtain a 2D delta function which is the image of a point scatterer.

Due to uncompensated motions, $R_t - R_o$ and $\dot{R}_t - \dot{R}_o$ will change over a large synthetic aperture interval. If this change is greater than the size of a resolution cell, the final reconstructed image is blurred.

To investigate this distortion in detail, let us assume that $\dot{R}_t - \dot{R}_o$ is a constant and take the inverse 1D Fourier transform of (3) with respect to $\hat{t}$ (this is called range compression). We have an array of 1D delta functions centered at positions proportional to $R_t - R_o$. If $R_t - R_o$ is a constant, then these delta functions are aligned in the range direction, so taking a second inverse 1D Fourier transform with respect to $n$ (this is called azimuth compression) will give a 2D delta function. However, since $R_t - R_o$ is not a constant, these delta functions are not aligned in the range direction. Taking the inverse 1D Fourier transform with respect to $n$ spreads the 2D delta function in both the range and the azimuth direction. Hence, considering the RFA processing as a linear system, the 2D spread delta function is indeed the impulse response of this system. In general, this system is shift-variant, which means, for scatterers at different locations in the scene, these impulse responses are different. However, if the size of a target is small, then different scatterers of the target will have a similar spreading pattern, while targets at different locations will have different spreading patterns.

### B. Distortion model

Based on the discussion in the previous subsection, we model the smeared target image as the superposition of different shifts (in space) of the focused target image. If the focused target signature function is $s(x,y)$, then the distorted target image is modeled by

$$s_d(x,y) = \sum_{k=1}^{K} \alpha_k s(x - x_k, y - y_k) \quad (4)$$

We illustrate that indeed this is the appropriate model by forming the image for the spotlight SAR geometry shown in Fig. 1. In the simulation, the pulse length $T_p$ is $4\mu$s, the center frequency $f_c$ is 242.4MHz, the chirp rate $\gamma$ is 33.375MHz/$\mu$s and the synthetic aperture length $L$ is 760.8m. The plot in Fig. 2 depicts the image of a rectangular target with 18 scatterers at the scene center. The image is formed using RFA. Since relative motions of scatterers at the scene center are fully compensated by dechirping, the plot shows an undistorted rectangular target. The plot in Fig. 3 shows the image of the same target located at (200m, 0). As seen from the plot, the distorted target consists of five translated replicas of the focused target image. This is because the relative motions of scatterers far from the scene center are not appropriately compensated by dechirping.

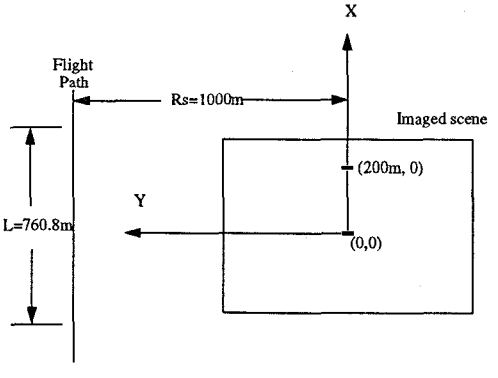


Fig. 1. Geometry

## III. Geometric approach

In this section, we discuss the target detection problem by utilizing the distortion model that we described in the

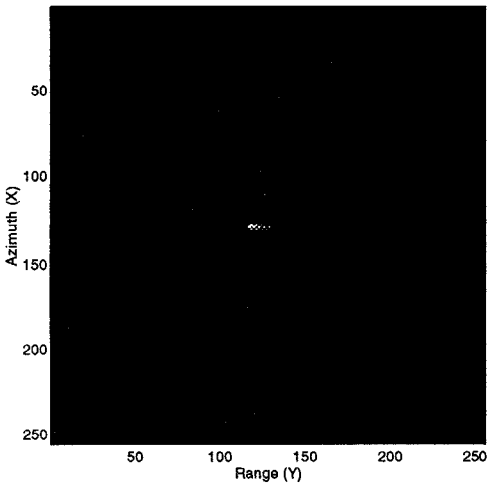


Fig. 2. Image of a rectangular target at the scene center (0,0).

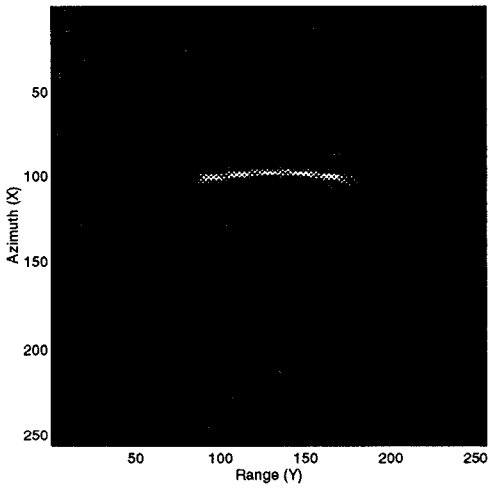


Fig. 3. Image of a rectangular target at (200m,0).

previous section.

### A. Detection formulation

The target detection problem is cast in the following hypothesis testing problem

$$H_1 : r(x,y) = \sum_{k=1}^{K} \alpha_k s(x-x_k, y-y_k) + n(x,y) \quad (5)$$

$$H_0 : r(x,y) = n(x,y) \quad (6)$$

where $s(x,y)$ is the focused target signature, $n(x,y)$ is the background noise, $K$ is the number of shifted (in space) replicas, $\alpha_k$ is the attenuation of the $k$th replica and $(x_k, y_k)$ is the space shift of the $k$th replica. In this paper, we assume that the focused target signature is known and the noise is white and Gaussian. We also assume that the distortion parameters: $\{(x_k, y_k)\}$, $\{\alpha_k\}$, and $K$ are deterministic unknown.

We describe our approach in the context of generalized likelihood ratio test (GLRT) detection[2]. It is based on a geometric interpretation of the detection problem. Let $\mathcal{S}$ be the signal subspace containing all the possible distorted target signatures for a given signal model, i.e.,

$$\mathcal{S} = \left\{ \sum_{k=1}^{K} \alpha_k s(x-x_k, y-y_k) \right\} \quad (7)$$

The GLRT test statistic is the energy of the orthogonal projection of $r(x,y)$ on the subspace $\mathcal{S}$, i.e.,

$$L = \| P_{\mathcal{S}}(r(x,y)) \|_2^2 \quad (8)$$

where $P_{\mathcal{S}}(r(x,y))$ is the orthogonal projection of $r(x,y)$ on $\mathcal{S}$ and $\| \cdot \|_2$ is the $L_2$ norm.

Calculating the orthogonal projection $P_{\mathcal{S}}(r(x,y))$ requires a costly multi-dimensional nonlinear optimization. Our approach is to approximate this orthogonal projection by designing a representation subspace $\mathcal{G}$ which satisfies three requirements:

- The orthogonal projection on $\mathcal{G}$ is easily computed;
- $\mathcal{G}$ is easily designed;
- The orthogonal projection on the representation subspace $\mathcal{G}$ is close to the orthogonal projection on $\mathcal{S}$ in the gap metric sense.

The gap metric [4] is a distance measure between two closed subspaces. Given two closed subspaces $\mathcal{S}$ and $\mathcal{G}$ in a Hilbert space $H$, we denote by $\mathcal{S}_S$ the unit sphere of $\mathcal{S}$ (the set of all $u \in \mathcal{S}$ with $\| u \|_2 = 1$) and let

$$\hat{\delta}(\mathcal{S}, \mathcal{G}) = \sup_{u \in \mathcal{S}_S} \mathrm{dist}(u, \mathcal{G}) \quad (9)$$

where $\mathrm{dist}(u, \mathcal{G}) = \inf_{v \in \mathcal{G}} \| u - v \|_2$. Likewise, we define $\hat{\delta}(\mathcal{G}, \mathcal{S})$. The quantity

$$\delta(\mathcal{S}, \mathcal{G}) = \max(\hat{\delta}(\mathcal{S}, \mathcal{G}), \hat{\delta}(\mathcal{G}, \mathcal{S})) \quad (10)$$

is called the gap between $\mathcal{S}$ and $\mathcal{G}$.

An equivalent perhaps more intuitive definition of the gap metric is also given in [4]. It is defined in terms of the orthogonal projection operators of $\mathcal{S}$ and $\mathcal{G}$. Denote by $P_{\mathcal{S}}$ and $P_{\mathcal{G}}$ the orthogonal projection operators of $\mathcal{S}$ and $\mathcal{G}$ respectively, then the gap metric is

$$\delta(\mathcal{S}, \mathcal{G}) = \| P_{\mathcal{S}} - P_{\mathcal{G}} \| \quad (11)$$

where $\| \cdot \|$ is the $L_2$ induced operator norm.

Once we have $\mathcal{G}$, the new test statistic is the energy of the orthogonal projection of the observation $r(x,y)$ on the representation subspace

$$\tilde{L} = \| P_{\mathcal{G}}(r(x,y)) \|_2^2 \quad (12)$$

*B. Subspace design*

In this subsection, we discuss the subspace design problem. Our goal is to find a representation subspace $\mathcal{G}$ that satisfies the three requirements described in the previous subsection. First of all, we choose $\mathcal{G}$ in the following form

$$\mathcal{G} = \left\{ \sum_{m,n=-\infty}^{+\infty} \beta_{m,n} g(x-m, y-n) \right\} \tag{13}$$

In general, subspace design is difficult. However, by choosing the subspace structure given in (13), we reduce the subspace design problem to a functional design problem. Now, we need only to design the function $g(x,y)$. Also, with this representation subspace structure, the orthogonal projection on $\mathcal{G}$ is easily computed by taking inner products.

We design the subspace $\mathcal{G}$ in two steps:

1. Design the representation subspace $\mathcal{G}$ to minimize the gap between $\mathcal{G}$ and an integer shifted subspace $\mathcal{S}_{int}$ of $\mathcal{S}$;
2. Reshape the optimal $g^*(x,y)$ from step 1 to make it nearly shiftable using the reshaping algorithm in [5].

We show that the gap between $\mathcal{S}_{int}$ and $\mathcal{G}$ is

$$\delta(\mathcal{S}_{int}, \mathcal{G}) = \sqrt{1 - \inf_{f_1, f_2 \in [0,1)} C_{sg}(f_1, f_2)} \tag{14}$$

where $C_{sg}(f_1, f_2)$ is

$$\frac{|\sum_{k,l} \mathcal{F}_s(f_1+k, f_2+l)\overline{\mathcal{F}_g(f_1+k, f_2+l)}|^2}{\sum_{m,n} |\mathcal{F}_s(f_1+m, f_2+n)|^2 \sum_{m,n} |\mathcal{F}_g(f_1+m, f_2+n)|^2} \tag{15}$$

where $\mathcal{F}_s(f_1, f_2)$ and $\mathcal{F}_g(f_1, f_2)$ are the Fourier transform of $s(x,y)$ and $g(x,y)$ respectively and $\overline{\mathcal{F}_g(f_1, f_2)}$ is the complex conjugate of $\mathcal{F}_g(f_1, f_2)$.

We further restrict $g(x,y)$ to be a 2D separable compactly supported orthonormal scaling function [6] so that we use the parameterization given in [7]. With the parameterization of $g(x,y)$, the functional design problem is reduced to a finite parameter optimization problem. Now, $C_{sg}(f_1, f_2)$ is a function of the parameter $\zeta$ that parameterizes $g(x,y)$. We write it explicitly as $C_{sg}(f_1, f_2, \zeta)$.

Minimizing $\delta(\mathcal{S}_{int}, \mathcal{G})$ is equivalent to maximizing

$$\inf_{f_1, f_2 \in [0,1)} C_{sg}(f_1, f_2, \zeta) \tag{16}$$

We carry out the maximization of (16) by doing a brute-force search of the parameter space. That is, we compute (16) at discrete sample points of $\zeta$ and pick the value $\zeta^*$ that maximizes (16). Then, we use an algorithm given in [8] to reconstruct the optimal scaling function $g^*(x,y)$ from $\zeta^*$.

In step 2, Benno and Moura's algorithm [5] is used to reshape the optimal $g^*(x,y)$ obtained from step 1 to make it nearly shiftable.

## IV. Simulation results

In this section, we present simulation results to demonstrate the performance of the robust detector for the 1D case.

We compare the performance of our robust detector with two other detectors: the correlator detector and the "Matched Filter with Integer Shifts" (MFIS) detector. The correlator detector is a simple detector. It correlates the observed target image with the focused target image and uses the information in the peaks of the correlator output to form the test statistic and detect the target. The MFIS detector is also a simple detector. It has the same structure as our robust detector. The difference is that, in the MFIS detector case, the observed target image is matched to the integer shifted replicas of the focused target image, while, in our robust detector case, the observed target image is matched to the integer shifts of the reshaped optimal scaling function $g^*(x,y)$ we design.

In the 1D case, we use the following equivalent distortion model

$$s_d(t) = \sum_{k=1}^{K} \alpha_k s(t - \tau_k) \tag{17}$$

We call $s(t)$ the transmitted signal which corresponds to the focused target signature $s(x,y)$ and call $\tau_k$ the delay which corresponds to the space shift $(x_k, y_k)$.

In the simulation, we pick the following signal as the transmitted signal

$$s(t) = \exp(-t) \cdot \cos(t) \cdot (u(t) - u(t-8)) \tag{18}$$

where $u(t)$ is the unit step function. The signal $s(t)$ is a truncated modulated decaying exponential with damping coefficient 1 and modulating frequency $1/2\pi$. The signal $s(t)$ is sampled at intervals $1/64$.

For simplicity, we set all the attenuation factors $\{\alpha_k\}$ to 1. The number of replicas $K$ is set to 15. We generate the delays $\{\tau_k\}$ using a random number generator. For a fixed pattern of delays, we calculate the probability of detection $P_D$ as a function of the signal-to-noise ratio (SNR) with fixed probability of false alarm probability $P_F$. Then, we repeat it 100 times to see how the performance changes with the delay patterns.

Fig. 4 shows the average detection probabilities as a function of the SNR with the false alarm probability $P_F = 0.01$. The solid line in the figure represents an unrealistic performance bound. It is the performance

curve obtained by assuming that all the delays are exactly known. Fig. 4 shows that our detector provides

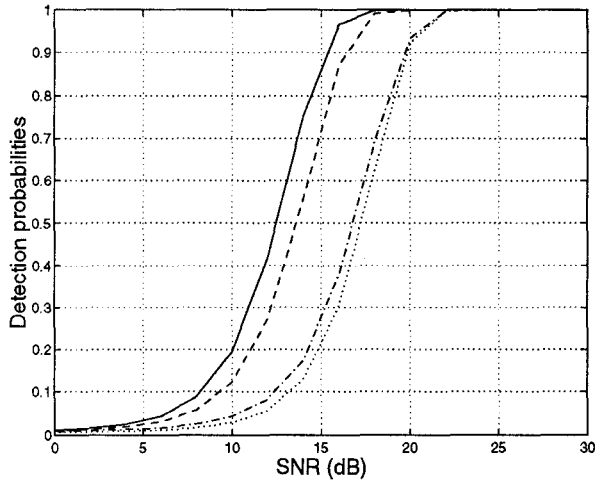


Fig. 4. The average detection probabilities, $K = 15$, $P_F = 0.01$. The solid line is a performance bound, "——" is the new robust detector, "–." is the correlator detector, and "···" is the MFIS detector.

about 3.5dB gain over the correlator detector and about 4dB gain over the MFIS detector. In this simulation, the MFIS detector is outperformed by other detectors. The potential maximum gain over the MFIS detector is given by the distance between the two extreme curves in Fig. 4, namely the left most curve corresponding to the optimistic upper bound and the right most curve corresponding to the MFIS detector. This gain is about 5 dB. We see from Fig. 4 that our robust detector is able to recover 80% of the potential gain.

The performance of our robust detector does not change significantly with the delay patterns. This phenomenon is demonstrated in Fig. 5. Fig. 5 depicts the detection probabilities at SNR = 18dB as a function of the delay patterns. We can see that the robust detector (top curve in the plot of Fig. 5) not only performs better than the correlator detector and the MFIS detector but also oscillates much less than these two detectors.

## V. Summary

In this paper, we describe a robust detection scheme for unfocused SAR/ISAR images. We show that the blurred and smeared target signature in SAR/ISAR images, which are due to the lack of relative motion compensation, can be equivalently modeled as the superposition of multiple space shifted replicas of the fully compensated target signature. Based on this distortion model, we extend our previous work to the 2D case to solve this problem. Our approach is to consider the distortion explicitly, rather than ignoring it. The detector matched

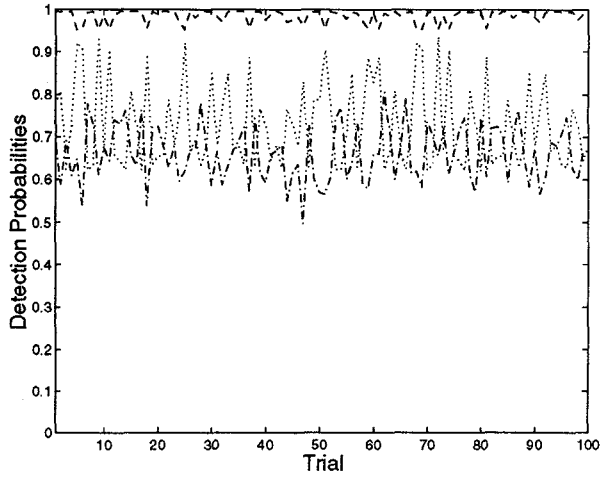


Fig. 5. Detection probabilities at 18dB for different delay patterns. "——" is our robust detector, "–." is the correlator detector, and "···" is the MFIS detector.

to this model is then robust to the distortion.

## References


[1] W. G. Carrara, R. S. Goodman, and R. Majewski, *Spotlight Sysnthetic Aperture Radar. Signal Processing Algorithms.* Artech House, 1995.

[2] C. He, J. M. F. Moura, and S. A. Benno, "Gap detector for multipath," in *ICASSP*, May 1996, pp. V-2650–2653.

[3] C. He and J. M. F. Moura, "Robust detection with the gap metric," *Submitted to IEEE Trans. on Signal Processing*, revised November 1996.

[4] T. Kato, *Perturbation theory for linear operators.* Springer Verlag, 2nd ed., 1976.

[5] S. A. Benno and J. M. F. Moura, "Nearly shiftable scaling functions," in *ICASSP*, May 1995, pp. II–1097–1100.

[6] S. Mallat, "A theory for multiresolution signal decomposition," *IEEE Trans. Patt. Anal. Mach. Intell.*, vol. 11, pp. 674–693, July 1989.

[7] H. Zou and A. H. Tewfik, "Parameterization of compactly supported orthonormal wavelets," *IEEE Trans. Signal Processing*, vol. 41, pp. 1428–1431, March 1993.

[8] C. K. Chui, *An Introduction to Wavelets.* Academic Press, 1992.